Detection of the Pulsar Wind Nebula HESS J1825-137 with the Fermi Large Area Telescope

M.-H. Grondin, S. Funk, M. Lemoine-Goumard, A. van Etten, J. A. Hinton, F. Camilo, Ismaël Cognard, C. M. Espinoza, P. C. C. Freire, J. E. Grove, et al.

The Astrophysical Journal, 738:42 (7pp), 2011 September 1 doi:10.1088/0004-637X/738/1/42

DETECTION OF THE PULSAR WIND NEBULA HESS J1825−137 WITH THE *FERMI* LARGE AREA TELESCOPE

M.-H. Grondin[1,12], S. Funk[2], M. Lemoine-Goumard[1], A. Van Etten[2], J. A. Hinton[3], F. Camilo[4], I. Cognard[5], C. M. Espinoza[6], P. C. C. Freire[7], J. E. Grove[8], L. Guillemot[7], S. Johnston[9], M. Kramer[6,7], J. Lande[2], P. Michelson[2], A. Possenti[10], R. W. Romani[2], J. L. Skilton[11], G. Theureau[5], and P. Weltevrede[6]

[1] Centre d'Études Nucléaires de Bordeaux Gradignan, Université Bordeaux 1, CNRS/IN2P3, 33175 Gradignan, France; grondin@cenbg.in2p3.fr, lemoine@cenbg.in2p3.fr
[2] W. W. Hansen Experimental Physics Laboratory, Kavli Institute for Particle Astrophysics and Cosmology, Department of Physics and SLAC National Accelerator Laboratory, Stanford University, Stanford, CA 94305, USA; funk@slac.stanford.edu, ave@stanford.edu
[3] Department of Physics and Astronomy, University of Leicester, Leicester LE1 7RH, UK
[4] Columbia Astrophysics Laboratory, Columbia University, New York, NY 10027, USA
[5] Laboratoire de Physique et Chimie de l'Environnement, LPCE UMR 6115 CNRS, F-45071 Orléans Cedex 02, and Station de radioastronomie de Nançay, Observatoire de Paris, CNRS/INSU, F-18330 Nançay, France
[6] Jodrell Bank Centre for Astrophysics, School of Physics and Astronomy, The University of Manchester, M13 9PL, UK
[7] Max-Planck-Institut für Radioastronomie, Auf dem Hügel 69, 53121 Bonn, Germany
[8] Space Science Division, Naval Research Laboratory, Washington, DC 20375, USA
[9] Australia Telescope National Facility, CSIRO, Epping, NSW 1710, Australia
[10] INAF-Cagliari Astronomical Observatory, I-09012 Capoterra (CA), Italy
[11] School of Physics and Astronomy, University of Leeds, Leeds LS2 9JT, UK
Received 2010 November 3; accepted 2011 May 25; published 2011 August 10

ABSTRACT

We announce the discovery of 1–100 GeV gamma-ray emission from the archetypal TeV pulsar wind nebula (PWN) HESS J1825−137 using 20 months of survey data from the *Fermi*-Large Area Telescope (LAT). The gamma-ray emission detected by the LAT is significantly spatially extended, with a best-fit rms extension of $\sigma = 0.^{\circ}56 \pm 0.^{\circ}07$ for an assumed Gaussian model. The 1–100 GeV LAT spectrum of this source is well described by a power law with a spectral index of $1.38 \pm 0.12 \pm 0.16$ and an integral flux above 1 GeV of $(6.50 \pm 0.21 \pm 3.90) \times 10^{-9}$ cm^{-2} s^{-1}. The first errors represent the statistical errors on the fit parameters, while the second ones are the systematic uncertainties. Detailed morphological and spectral analyses bring new constraints on the energetics and magnetic field of the PWN system. The spatial extent and hard spectrum of the GeV emission are consistent with the picture of an inverse Compton origin of the GeV–TeV emission in a cooling-limited nebula powered by the pulsar PSR J1826−1334.

Key words: gamma rays: general – ISM: individual objects (G18.0-0.7, HESS J1825−137) – pulsars: general – pulsars: individual (PSR B1823–13, PSR J1826–1334)

Online-only material: color figures

1. INTRODUCTION

Pulsars dissipate their energy via magnetized particle winds (consisting of electron/positron pairs) with the confinement of this particle wind outflow leading to the phenomenon of pulsar wind nebulae (PWNe). PWNe develop when the particle wind collides with its surroundings, in particular with the slowly expanding supernova ejecta, and form a termination shock. Even though many PWNe are bright enough to be resolvable both spatially and spectrally at wavelengths from radio to very high energy (VHE; $E > 100$ GeV) gamma rays, many open questions remain. How is the rotational energy of the pulsar converted into a relativistic particle wind? What is the bulk Lorentz factor of the wind, what is the mechanism by which the particles are accelerated at the termination shock? What is the partition between magnetic and particle energy in the wind? To address these questions, PWNe can be seen as laboratories for relativistic astrophysics with the advantage of having a well-localized (and usually well-characterized) central energy source, the spin-down power of a neutron star.

Many studies of PWNe have been conducted in the X-ray band with instruments such as *XMM-Newton* or *Chandra* (Kargaltsev & Pavlov 2008), but recent gamma-ray observations with H.E.S.S., MAGIC, and VERITAS have contributed significantly to the understanding of PWNe. Together with the assumption that the X-ray emission is synchrotron whereas the higher energies are inverse Compton (IC) emission, these observations allow us to derive the magnetic field strength in the nebula. For the PWNe seen in TeV gamma rays, typical magnetic field strengths are $\sim$10 μG (de Jager & Djannati-Ataï 2009). In turn, the lifetime of the synchrotron-emitting electrons can be determined from the magnetic field strengths. For keV X-ray emitting electrons the lifetime of less than 100 years is significantly shorter than the age of the central pulsar (10^3–10^5 years), whereas the TeV emitting electrons have lifetimes of order 10^4 years, comparable to the pulsar age. This has the consequence that the X-ray PWNe should be spatially very compact, whereas the PWNe as seen in TeV should be significantly larger. The discovery of energy-dependent morphology at TeV energies in the archetypal system HESS J1825−137 (surrounding the energetic pulsar PSR J1826−1334) confirmed this basic picture by demonstrating that the emission is dominated by "relic" electrons from the earlier epochs of the nebula in which the pulsar was spinning down more rapidly, releasing more energy into the system (Aharonian et al. 2006). The gamma-ray studies of PWNe also showed that the overall efficiency of conversion

[12] Current address: Institut für Astronomie und Astrophysik Tübingen, Universität Tübingen, Sand 1, D-72076 Tübingen, Germany.

of rotational energy into TeV emission in these systems is extremely high ($\gg$10% in some cases).

The recently launched Large Area Telescope (LAT) on board the *Fermi Gamma-ray Space Telescope* has established pulsars as the most numerous class of identified Galactic GeV gamma-ray emitting objects (Abdo et al. 2010b) and has also shown that up to 10% of the rotational power from pulsars is emitted in the *Fermi*-LAT energy band. The spectrum of the pulsed component cuts off in the sub-10-GeV range (Abdo et al. 2010a). As detailed above, the spectra of PWNe extend out to TeV energies making PWNe the most numerous Galactic objects at those energies. While for a few TeV sources there is a clear morphological match (e.g., with the X-ray emission) that leads to the identification with a PWN, for most TeV sources the situation is less obvious. Generally, a positional match with a pulsar (along with the requirement that the energetics of the pulsar is sufficient to power the TeV emission) is used to suggest an association. The situation is, however, further complicated by the fact that for many of the TeV-detected PWNe, in particular for the ones that are associated with middle-aged rather than young pulsars, the gamma-ray emission is offset from the pulsar.

HESS J1825−137 is one of the prime examples for such an offset PWN system. The system seems to be powered by the energetic radio pulsar PSR J1826−1334. High-resolution X-ray observations of the PWN with *XMM-Newton* showed a compact core with a hard photon index ($\Gamma = 1.6^{+0.1}_{-0.2}$) of size 30″ embedded in a larger diffuse structure of extension ∼5′ extending to the south of the pulsar with a softer photon index of $\Gamma \sim 2.3$ (Gaensler et al. 2003). The TeV gamma-ray emission has a much larger extent (∼0.°5) and shows a similar softening of the photon index from $\Gamma = 2.0$ close to the pulsar to $\Gamma = 2.5$ at a distance of 1° to the south of the pulsar (Aharonian et al. 2006). Based on hydrodynamical simulations (Blondin et al. 2001) the asymmetric nature of the emission can be explained by dense interstellar material to the north of the pulsar. The reverse shock of the supernova explosion from that direction might have been pushed inward, interacting therefore relatively early with the PWN and thus pushing the X-ray and TeV gamma-ray emission mainly to the south.

Here, we report on GeV gamma-ray observations of the HESS J1825−137/PSR J1826−1334 system with *Fermi*-LAT.

2. LAT DESCRIPTION AND OBSERVATIONS

The LAT is a gamma-ray telescope that detects photons by conversion into electron–positron pairs and operates in the energy range between 20 MeV and more than 300 GeV. It is made of a high-resolution converter tracker (for direction measurement of the incident gamma rays), a CsI(Tl) crystal calorimeter (for energy measurement), and an anti-coincidence detector to identify the background of charged particles (Atwood et al. 2009). In comparison to EGRET, the LAT has a larger effective area (∼8000 cm^2 on-axis above 1 GeV), a broader field of view (∼2.4 sr), and a superior angular resolution (∼0.°6, 68% containment at 1 GeV for events converting in the front section of the tracker). Details of the instrument and data processing are given in Atwood et al. (2009). The on-orbit calibration is described in Abdo et al. (2009a).

The following analysis was performed using 20 months of data collected starting 2008 August 4 and extending until 2010 April 21. Only gamma rays in the Pass 6 *Diffuse* class events were selected (i.e., with the tightest background rejection), and from this sample, we excluded those coming from a zenith angle larger than 105° to the detector axis because of the possible contamination from secondary gamma rays from Earth's atmosphere (Abdo et al. 2009b). We have used P6_V3 post-launch instrument response functions (IRFs), which take into account pile-up and accidental coincidence effects in the detector subsystems.

3. TIMING ANALYSIS OF THE PULSAR PSR J1826−1334

The pulsar PSR J1826−1334 (also known as PSR B1823−13) was discovered in the survey of Clifton et al. (1992). Its spin period of 101.48 ms, characteristic age of 21 kyr, and spin-down power of 2.8×10^{36} erg s^{-1} are very similar to those of the Vela pulsar. The distance to the pulsar as derived from the dispersion measure is (3.9 ± 0.4) kpc (Cordes & Lazio 2002). Although the pulsar was not reported in the *Fermi*-LAT catalog of gamma-ray pulsars with 6 months of data (Abdo et al. 2010a), we performed a temporal analysis on this increased *Fermi*-LAT data set using a new timing solution. A total of 162 observations of PSR J1826−1334 were made at 1.4 GHz using the Parkes (Weltevrede et al. 2010), Lovell (Hobbs et al. 2004), and Nançay (Cognard et al. 2010) radio telescopes. The TEMPO2 timing package (Hobbs et al. 2006) was then used to build the timing solution. We fit the radio times of arrival to the pulsar rotation frequency and first three derivatives. We whitened the timing noise with four harmonically related sinusoids, using the "FITWAVES" functionality of the TEMPO2 package. The post-fit rms is 292.4 μs, or 0.2% of the pulsar phase. This timing solution will be made available through the Fermi Science Support Center (FSSC).[13]

Photons with an angle $\theta < \max(5.°12 \times (E/100\,\mathrm{MeV})^{-0.8}, 0.°2)$, where E is the energy of the photon, from the radio pulsar position, R.A. = 276.°55490, decl. = −13.°57967 (J2000), were selected and phase-folded using the above-mentioned ephemeris. The energy dependence of the integration radius is a satisfactory approximation of the shape of the LAT point-spread function (PSF), especially at low energies.

The H-test values, as defined in de Jager et al. (1989) and obtained from the analysis of the pulsed emission, correspond to a significance well below 2σ for each tested energy band (30 MeV–300 GeV, 30–100 MeV, 100–300 MeV, 300 MeV–1 GeV, >1 GeV). No significant pulsation is detected with the current statistics. We fitted a point source at the position of the pulsar PSR J1826−1334 and derived an upper limit between 100 MeV and 1 GeV of $\sim 3.1 \times 10^{-8}$ cm^{-2} s^{-1}, well below typical gamma-ray fluxes reported for pulsars detected by *Fermi*-LAT (Abdo et al. 2010a). This ensures that any emission from the PWN HESS J1825−137 will not be contaminated by pulsed gamma-ray photons from PSR J1826−1334.

4. ANALYSIS OF THE PULSAR WIND NEBULA HESS J1825−137

The spatial and spectral analysis of the gamma-ray emission was performed using two different methods, *gtlike* and *Sourcelike*. *gtlike* is the maximum-likelihood method (Mattox et al. 1996) implemented in the FSSC science tools. This tool fits a source model to the data along with models for the instrumental, extragalactic, and Galactic backgrounds. In the following spectral analysis, the Galactic diffuse emission is modeled using the ring-hybrid model *gll_iem_v02.fit*. The instrumental background and the extragalactic radiation are described by a single isotropic component with a spectral shape described by the

[13] FSSC: http://fermi.gsfc.nasa.gov/ssc/data/access/lat/ephems/.

Table 1
Centroid and Extension Fits to the LAT Data for HESS J1825−137 Using *Sourcelike* for Events with Energies Above 10 GeV

Model	Name	$l(^\circ)$	$b(^\circ)$	Radius (°)	TS_{ext}
Point source	PS	17.62	−0.82		
Disk	*D*	17.57	−0.45	0.67 ± 0.02	72
Gaussian	*G*	17.57	−0.43	0.56 ± 0.07	72

Note. The difference in test statistic between a given spatial model and the point-source hypothesis is indicated by TS_{ext} in the last column.

tabulated model *isotropic_iem_v02.txt*. The models and their detailed description are released by the LAT Collaboration.[14] Sources within 10° of the pulsar PSR J1826−1334 and found above the background with a statistical significance larger than 5σ are extracted from the source list given in Abdo et al. (2010b), except for 1FGL J1825.7−1410c which contributes partially to the gamma-ray emission of the PWN. A detailed analysis reveals that the GeV emission is significantly extended compared with that of a point source. The morphological analysis was performed using *Sourcelike*, which is described in the Appendix. The extension test was done using a uniform disk and a Gaussian spatial model. *Sourcelike* can also be used to assess the test statistic (TS) value and to compute the spectra of both extended and point-like sources. The TS is defined as twice the difference between the log-likelihood L_1 obtained by fitting a source model plus the background model to the data, and the log-likelihood L_0 obtained by fitting the background model only, i.e., $TS = 2(L_1–L_0)$.

4.1. Morphology

To study the morphology of an extended source, a major requirement is to have the best possible angular resolution. Therefore, we decided to restrict our LAT data set to events with energies above 10 GeV. This also reduces the relative contribution of the Galactic diffuse background. Figure 1 (top) presents the LAT counts map of gamma-ray emission around HESS J1825−137, smoothed with a Gaussian of $\sigma = 0.^\circ35$. The image contains emission from the Galactic diffuse background and from nearby sources but in addition shows bright emission south of PSR J1826−1334 coinciding generally with the region that is bright at TeV energies (denoted by the H.E.S.S. flux contours). The TS map above 10 GeV presented in Figure 1 (bottom) supports this picture. This skymap contains the TS value for a point source at each map location, thus giving a measure of the statistical significance for the detection of a gamma-ray source in excess of the background. Clearly, significant emission to the south of PSR J1826−1334 is detected.

We determined the source extension using *Sourcelike* with a uniform disk hypothesis and a Gaussian distribution (compared to the point-source hypothesis). The results of the extension fits and the improvement of the TS when using spatially extended models are summarized in Table 1. The difference in TS between the Gaussian distribution and the point-source hypothesis is $TS_{ext} = 72$ (which converts into a significance of $\sim 8\sigma$ for the source extension) for 10 GeV $< E <$ 100 GeV, which demonstrates that the source is significantly extended with respect to the LAT PSF. The fit extension has a dispersion of $\sigma = 0.^\circ56 \pm 0.^\circ07$. We support this conclusion in Figure 2, showing the background subtracted radial profile for the LAT

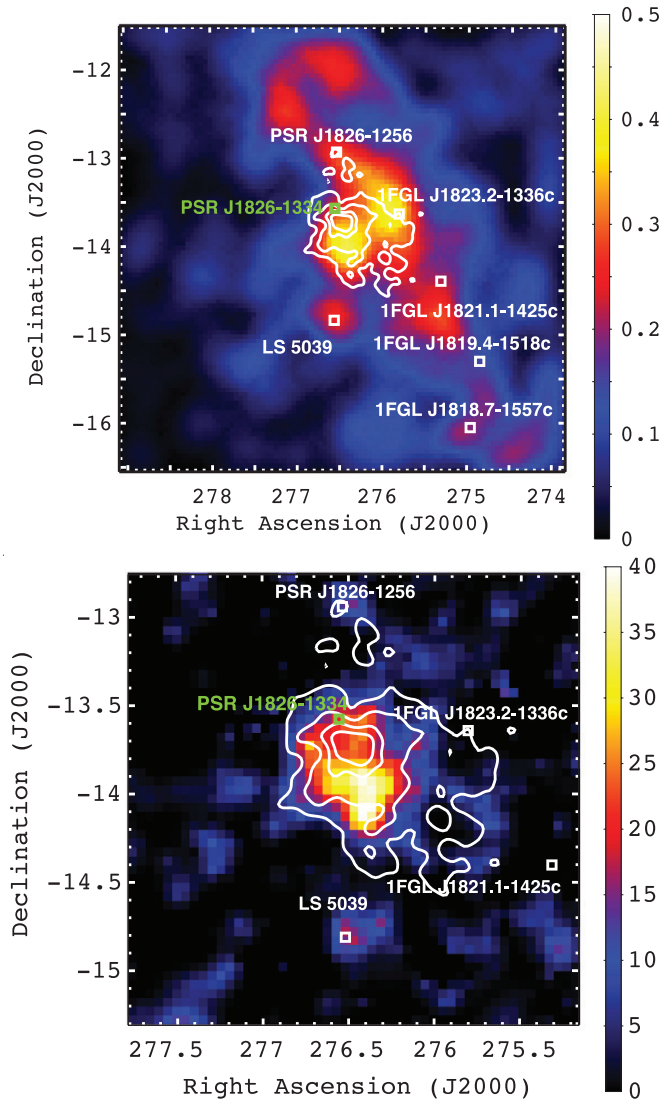

Figure 1. Top: *Fermi*-LAT counts map above 10 GeV of the HESS J1825−137 region with side length 5°, binned in square pixels of side length $0.^\circ05$. The map is smoothed with a Gaussian of $\sigma = 0.^\circ35$. H.E.S.S. contours (Aharonian et al. 2006) are overlaid as gray solid lines. The positions of the pulsar PSR J1826−1334 and of the close-by 1FGL sources are indicated with green and white squares, respectively. LS 5039 is visible in the southeast at position (R.A., decl.) = ($276.^\circ56$, $-14.^\circ85$). Bottom: *Fermi*-LAT test statistic (TS) map for events with energy larger than 10 GeV on a region of $2.^\circ5$ side length. The TS was evaluated by placing a point source at the center of each pixel, Galactic diffuse emission and nearby sources being included in the background model.
(A color version of this figure is available in the online journal.)

data above 10 GeV (from the best-source location determined for a Gaussian fit) and comparing this with the LAT PSF. Similar results are obtained assuming a uniform disk model.

We have also examined the correlation of the gamma-ray emission with different source morphologies by using *gtlike* with assumed multi-frequency templates. For this exercise we compared the TS of the point source and Gaussian distribution parameters provided by *Sourcelike* with values derived when using the H.E.S.S. gamma-ray excess map as a morphological template (Aharonian et al. 2006). The resulting TS values obtained from our maximum-likelihood fitting are summarized in Table 2. Fitting a uniform disk to the data using the best location and size provided by *Sourcelike* instead of a point-source hypothesis results in $TS_{ext} = 67$, comparable to the

[14] FSSC: http://fermi.gsfc.nasa.gov/ssc/.

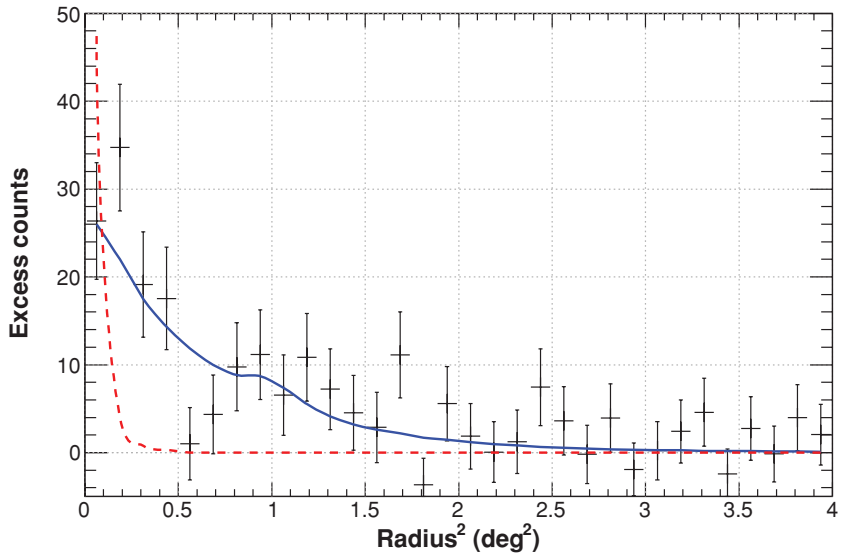

Figure 2. Background subtracted radial profile of the LAT data from the best-fit position provided by *Sourcelike* for a Gaussian source $(l, b) = (17.^\circ57, -0.^\circ43)$ as reported in Table 1 ($E > 10$ GeV). The best-fit model, obtained for a Gaussian distribution, and the LAT PSF are overlaid as a blue solid and a red dashed line, respectively, for comparison. The black dots represent the difference between the observed counts and the Galactic and extragalactic diffuse emission model. Nearby sources are not subtracted from the radial profile.

(A color version of this figure is available in the online journal.)

Table 2
Comparison of Model Likelihood Fitting Results with *gtlike* for Events with Energies Above 1 GeV

Model	Name	TS
Point source	PS	24
Disk	*D*	91
Gauss	*G*	104
H.E.S.S.		62

Note. For each model, we give the name and the test statistic value (TS).

improvement in TS between *D* and PS models in Table 1. Fitting a Gaussian model improves the TS by 80. Replacing the Gaussian with spatial template provided by the H.E.S.S. observations decreases the TS with respect to the Gaussian hypothesis ($\Delta TS = -42$), implying that the LAT emission is not perfectly reproduced by the H.E.S.S. excess map ($E >$ 200 GeV). This is not completely surprising since H.E.S.S. reported an energy-dependent morphology for this source and *Fermi* is probing lower energy electrons. Thus, while the best match is with the Gaussian morphology, we cannot rule out a simple disk morphology.

4.2. Spectral Analysis

The following spectral analyses are performed using *gtlike*. The *Fermi*-LAT spectral points were obtained by dividing the 1–100 GeV range into six logarithmically spaced energy bins and performing a maximum-likelihood spectral analysis in each interval, assuming a power-law shape for the source. For this analysis we used the Gaussian model from Table 1 to represent the gamma-ray emission observed by the LAT, as discussed in Section 4.1. Assuming this spatial shape, the gamma-ray source observed by the LAT is detected with a TS of 104 ($\sim 10\sigma$) in the 1–100 GeV range. To determine the integrated gamma-ray flux we fit a power-law spectral model to the data in the energy range 1–100 GeV with a maximum-likelihood analysis. This analysis is more reliable than a direct fit to the spectral points since it accounts for Poisson statistics of the data. The spectrum of HESS J1825−137 between 1 and 100 GeV, assuming the Gaussian model from Table 1, is presented in Figure 3. It is well described by a power law with a spectral index of $1.38 \pm 0.12 \pm 0.16$ and an integral flux above 1 GeV of $(6.50 \pm 0.21 \pm 3.90) \times 10^{-9}$ cm^{-2} s^{-1}. This is in agreement with results obtained independently using *Sourcelike*. The first error is statistical, while the second represents our estimate of systematic effects as discussed below and is dominated by the uncertainties on the Galactic diffuse emission in the 1–5 GeV energy range. With the current statistics, neither indication of a spectral cutoff at high energy nor significant emission below 1 GeV can be detected.

Four different systematic uncertainties can affect the LAT flux estimation: uncertainties on the Galactic diffuse background, on the morphology of the LAT source, on the effective area, and on the energy dispersion. The fourth one is relatively small ($\leqslant 10\%$) and has been neglected in this study. The main systematic at low energy is due to the uncertainty in the Galactic diffuse emission since HESS J1825−137 is located only $0.^\circ7$ from the Galactic plane. Different versions of the Galactic diffuse emission, generated by GALPROP (Strong et al. 2004), were used to estimate this error. The observed gamma-ray intensity of nearby source-free regions on the galactic plane is compared with the intensity expected from the galactic diffuse models. The difference, namely the local departure from the best-fit diffuse model, is found to be $\leqslant 6\%$ (Abdo et al. 2010e). By changing the normalization of the Galactic diffuse model artificially by $\pm 6\%$, we estimate the systematic error on the integrated flux of the PWN to be 70% below 5 GeV, 34% between 5 and 10 GeV, and $<12\%$ above 10 GeV. The second systematic is related to the morphology of the LAT source. The fact that we do not know the true gamma-ray morphology introduces another source of error that becomes significant when the size of the source is larger than the PSF, i.e., above 600 MeV for the case of HESS J1825−137. Different spatial shapes have been used to estimate this systematic error: a disk, a Gaussian distribution,

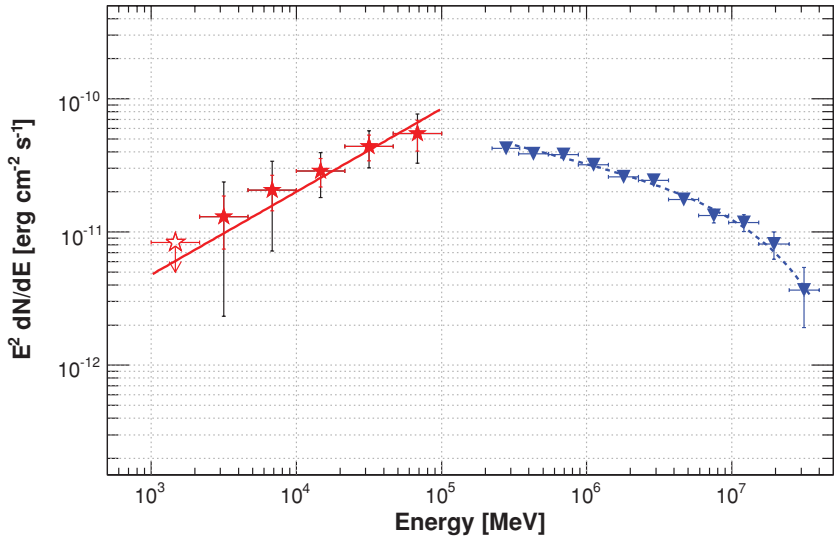

Figure 3. Spectral energy distribution of HESS J1825−137 in gamma rays. The LAT spectral points (in red) are obtained using the maximum-likelihood method *gtlike* described in Section 4.2 in six logarithmically spaced energy bins. The statistical errors are shown in red, while the black lines take into account both the statistical and systematic errors as discussed in Section 4.2. The red solid line presents the result obtained by fitting a power law to the data in the 1–100 GeV energy range using a maximum-likelihood fit. A 95% C.L. upper limit is computed when the statistical significance is lower than 3σ. The H.E.S.S. results are represented in blue (Aharonian et al. 2006).

(A color version of this figure is available in the online journal.)

and the H.E.S.S. template. Our estimate of this uncertainty is ∼30% above 1 GeV. The third uncertainty, common to every source analyzed with the LAT data, is due to the uncertainties in the effective area. This systematic is estimated by using modified IRFs whose effective area bracket that of our nominal IRF. These "biased" IRFs are defined by envelopes above and below the nominal dependence of the effective area with energy by linearly connecting differences of (10%, 5%, 20%) at log(E) of (2, 2.75, 4), respectively. We combine these various errors in quadrature to obtain our best estimate of the total systematic error at each energy and propagate through to the fit model parameters.

5. DISCUSSION

A one-zone spectral energy distribution (SED) model provides a useful tool to investigate the global properties of the PWN. Indeed, a number of recent papers have applied various one-zone models to investigate the broadband emission from PWNe (Lemiere et al. 2009; Gelfand et al. 2009; Bucciantini et al. 2011; Fang & Zhang 2010; Slane et al. 2010; Tanaka & Takahara 2010). Of particular interest, Fang & Zhang (2010) as well as Slane et al. (2010) applied the detailed model of Gelfand et al. (2009) and added a Maxwellian component to the electron spectrum.

HESS J1825−137 is non-uniform in the VHE regime (∼1° at 1 TeV and ∼0.°2 at 20 TeV) and possesses a bright central X-ray core observed with *Chandra* (Pavlov et al. 2008), *XMM-Newton* (Gaensler et al. 2003), and *Suzaku* (Uchiyama et al. 2009) which extends no more than 15′ from the pulsar. The non-uniform X-ray and VHE morphologies likely stem from cooling losses by energetic electrons as they traverse the nebula, yet at lower energies in the uncooled regime the electron spectral shape remains essentially constant with time, and hence also with position. As a result, even though a one-zone model cannot reproduce the energy-dependent morphology of the nebula, a one-zone model can nevertheless accurately reproduce the global flux from uncooled electrons. Electrons IC scattering off the cosmic microwave background (CMB) require energies of ∼2 TeV in order to produce photons of mean energy 10 GeV in the midst of the LAT energy range. Even in a 10 μG magnetic field such electrons' synchrotron cool quite slowly over a timescale of ∼45 kyr, roughly double the characteristic age of the pulsar. Inspection of Figure 3 indicates a spectral break at ∼200 GeV, almost certainly due to a cooling break in the electron spectrum. The hard LAT spectrum is therefore clearly in the uncooled regime, and so a one-zone model can help illuminate this new data.

We apply a one-zone time-dependent SED model, as described in Abdo et al. (2010c). This model computes SEDs from evolving electron populations over the lifetime of the pulsar in a series of time steps, with the energy content of the injected particle population varying with time following the pulsar spin down. During the free-expansion phase of the PWN (assumed to be $\sim 10^4$ years) we adopt an expansion of $R \propto t$, following which the radius $R \propto t^{0.3}$, appropriate for a PWN expanding in pressure equilibrium with a Sedov phase supernova remnant. Over the pulsar lifetime the magnetic field $B \propto t^{-0.5}$, following ∼500 years of constancy. At each time-step synchrotron, IC (Klein–Nishina effects included), and adiabatic losses are calculated. Synchrotron and IC fluxes are calculated from the final electron spectrum. We allow the braking index n of the pulsar to vary, thereby changing the age and spin-down behavior of the pulsar.

We assume the existence of three primary photon fields (CMBR, far-IR (dust), and starlight) and use the interstellar radiation mapcube within the GALPROP suite (Porter & Strong 2005) to estimate the photon fields at the Galactic radius of PSR J1826−1334. A distance of 3.9 kpc in the direction of the pulsar corresponds to a Galactic radius of 4.7 kpc. At this radius, the peak of the SED of dust IR photons corresponds to a black body temperature of $T \sim 32$ K with a density of ∼0.9 eV cm^{-3}, while the SED of stellar photons peaks at $T \sim 2500$ K with a density of ∼3.6 eV cm^{-3}.

Spectral measurements consist of LAT and H.E.S.S. data points, as well as an estimate of the X-ray spectrum. We adopt

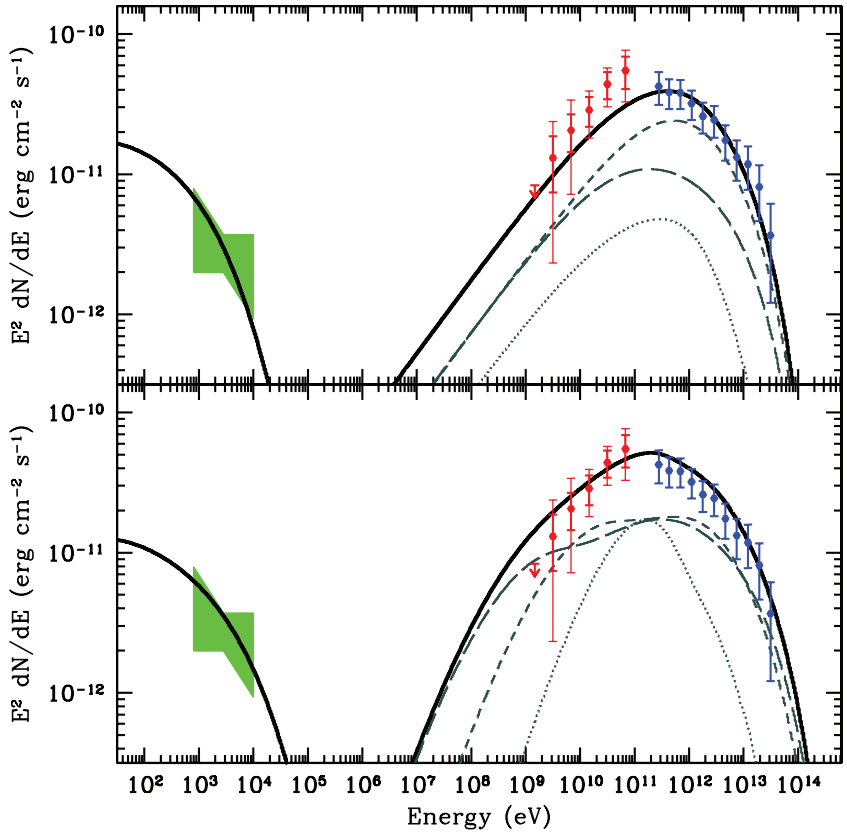

Figure 4. Spectral energy distribution of HESS J1825−137 with a simple exponentially cutoff power-law electron spectrum (top) and a relativistic Maxwellian plus power-law electron spectrum (bottom). The LAT spectral points (red, thin lines denote systematic errors) H.E.S.S. points (blue), and X-ray bowtie (green) are shown. The black line denotes the total synchrotron and IC emission from the nebula. Thin curves indicate the Compton components from scattering on the CMB (long-dashed), IR (medium-dashed), and stellar (dotted) photons.

(A color version of this figure is available in the online journal.)

an X-ray photon index of 2.2 ± 0.3 and a flux of $(7 \pm 2) \times 10^{-12}$ erg cm^{-2} s^{-1}. The selected index is consistent with the indices measured by *XMM-Newton* (Gaensler et al. 2003) and *Suzaku* (Uchiyama et al. 2009) for the extended nebula. The flux level is equivalent to sum of all the *Suzaku* regions analyzed by Uchiyama et al. (2009), with 30% systematic errors assumed.

A simple exponentially cutoff power-law injection of electrons, evolved properly over the pulsar lifetime, often provides an adequate match to PWNe SEDs. Initially, we fit this injection spectrum with four variables: final magnetic field, electron high-energy cutoff, electron power-law index, and the pulsar braking index n. Given the large covariance between the braking index and the initial spin period in determining the age of the pulsar, we fix the initial spin period at 10 ms and braking index at 2.5, yielding an age of 26 kyr for the system. This simple injection spectrum slightly underestimates the LAT data but the overall fit is still reasonable. For the source age of 26 kyr, we require a power-law index of 1.9, a cutoff at 57 TeV, and a magnetic field of 4 μG. The corresponding result is presented in Figure 4 (top).

Another option to fit the multi-wavelength data is adopting the relativistic Maxwellian plus power-law tail electron spectrum proposed by Spitkovsky (2008). For this injection spectrum, we assume a bulk gamma factor (γ_0) for the PWN wind upstream of the termination shock. At the termination shock the ambient pressure balances the wind pressure, fully thermalizing the wind; in this case, the downstream post-shock flow has $\gamma = (\gamma_0 - 1)/2$. One could also interpret this as an effective temperature kT of $m_e c^2 (\gamma_0 - 1)/2$. As per the simulations of Spitkovsky (2008), a power-law tail begins at $7kT \sim 7/2 m_e c^2 \gamma_0$ and suffers an exponential cutoff at some higher energy. For our modeling we fix the power law beginning at $\sim 7kT$, and allow kT, the power-law index, and the exponential cutoff to vary. The best fit, presented in Figure 4 (bottom), is obtained with $kT = 0.14$ TeV, corresponding to an upstream gamma factor of 5.5×10^5, a magnetic field of 3 μG, a cutoff at 150 TeV, and a power-law index of 2.3 close to the value of $\sim$2.5 proposed by Spitkovsky (2008). The relativistic Maxwellian plus power-law model matches the multi-wavelength data and also directly probes the upstream pulsar wind via fitting of γ_0.

HESS J1825−137 is detected at high significance by the *Fermi*-LAT, and demonstrates both morphological similarity and flux continuity with the H.E.S.S. regime. The LAT spectral index of $1.38 \pm 0.12 \pm 0.16$ is consistent with both a simple power-law electron injection spectrum, as well as a Maxwellian plus power-law injection spectrum over a simple power law. A mean magnetic field of $\sim$3–4 μG adequately fits the X-ray flux, and an age of $\sim$26 kyr is consistent with the data. A total of 5×10^{49} erg injected in the form of electrons by the pulsar is required to match the gamma-ray flux in the nebula.

The *Fermi*-LAT Collaboration acknowledges generous ongoing support from a number of agencies and institutes that have supported both the development and the operation of the LAT as well as scientific data analysis. These include the National Aeronautics and Space Administration and the Department of Energy in the United States, the Commissariat à l'Energie Atomique and the Centre National de la Recherche Scientifique/Institut

National de Physique Nucléaire et de Physique des Particules in France, the Agenzia Spaziale Italiana, the Istituto Nazionale di Fisica Nucleare, and the Istituto Nazionale di Astrofisica in Italy, the Ministry of Education, Culture, Sports, Science and Technology (MEXT), High Energy Accelerator Research Organization (KEK) and Japan Aerospace Exploration Agency (JAXA) in Japan, and the K. A. Wallenberg Foundation and the Swedish National Space Board in Sweden. Additional support for science analysis during the operations phase from the following agencies is also gratefully acknowledged: the Instituto Nazionale di Astrofisica in Italy and the Centre National d'Études Spatiales in France.

The Nançay Radio Observatory is operated by the Paris Observatory associated with the French Centre National de la Recherche Scientifique (CNRS).

The Lovell Telescope is owned and operated by the University of Manchester as part of the Jodrell Bank Centre for Astrophysics with support from the Science and Technology Facilities Council of the United Kingdom.

The Parkes radio telescope is part of the Australia Telescope which is funded by the Commonwealth Government for operation as a National Facility managed by CSIRO. We thank our colleagues for their assistance with the radio timing observations.

APPENDIX

DESCRIPTION OF *Sourcelike*

Sourcelike is a tool developed for performing morphological studies of spatially extended *Fermi* sources. *Sourcelike* is an extension to *pointfit* (described in Abdo et al. 2010b), which was developed to efficiently create TS maps and localize catalog sources with little sacrifice of precision. *pointfit* bins the sky in position and energy, and increases efficiency by scaling the spatial bin size with energy. Furthermore, it uses a region of the sky centered on the source whose radius is energy dependent: from 15° at 100 MeV to 3.°5 at 50 GeV. It was successfully used by and is described in the 1FGL catalog (Abdo et al. 2010b). *Sourcelike* deviates from *pointfit* by fitting not the PSF but the PSF convolved with an assumed spatial shape. By independently fitting the flux in each energy bin, *Sourcelike* performs an extension analysis without biasing the fit by assuming a spectral model. Since the PSF ranges a full two orders of magnitude in size over the energy range of the instrument, this maximum-likelihood approach naturally handles the energy-dependent PSF and maximizes our sensitivity to extension.

To find the shape of the source that most closely matches the observed photons, the overall likelihood is maximized by simultaneously fitting the spatial parameters of the source. At each step in the fit, the new shape must be again convolved with the PSF. It is for this reason that this optimized software was developed. Errors on the fit position and extension are estimated by numerically calculating the curvature of the likelihood function at the best-fit spatial model. The statistical significance of a source's extension is computed by *Sourcelike* by calculating TS_{ext}, which is defined as twice the difference between the log-likelihood L_1 obtained by fitting as an extended source and the log-likelihood L_0 obtained by fitting as a point source, i.e., $TS = 2(L_1 - L_0)$. The statistical significance of a source's extension is then calculated as $\sqrt{TS_{ext}}$. *Sourcelike* is particularly well suited for extension studies. It was extensively tested and validated against *gtlike*, and has been used in other LAT studies of PWNe (Abdo et al. 2010c, 2010d).

REFERENCES

Abdo, A. A., et al. 2009a, ApJ, 696, 1084
Abdo, A. A., et al. 2009b, Phys. Rev. D, 80, 122004
Abdo, A. A., et al. 2010a, ApJS, 187, 460
Abdo, A. A., et al. 2010b, ApJS, 188, 405
Abdo, A. A., et al. 2010c, ApJ, 713, 146
Abdo, A. A., et al. 2010d, ApJ, 714, 927
Abdo, A. A., et al. 2010e, ApJ, 722, 1303
Aharonian, F., et al. 2006, A&A, 460, 365
Atwood, W. B., et al. 2009, ApJ, 697, 1071
Blondin, J. M., Chevalier, R. A., & Frierson, D. M. 2001, ApJ, 563, 806
Bucciantini, N., Arons, J., & Amato, E. 2011, MNRAS, 410, 381
Clifton, T. N., Lyne, A. G., Jones, A. W., McKenna, J., & Ashworth, M. 1992, MNRAS, 254, 177
Cognard, I., Theureau, G., Desvignes, G., & Ferdman, R. 2010, in Proc. XXIst Rencontres de Blois, Nançay as Part of the International Pulsar Timing Campaigns, ed. L. Celnikier, J. Dumarchez, & J. Tran Thanh Van (Vietnam: The Gioi Publishers), 555
Cordes, J. M., & Lazio, T. J. W. 2002, arXiv:astro-ph/0207156
de Jager, O. C., & Djannati-Ataï, A. 2009, Neutron Stars and Pulsars (Astrophysics Space Science Library, Vol. 357; Berlin: Springer), 451
de Jager, O. C., Raubenheimer, B. C., & Swanepoel, J. W. H. 1989, A&A, 221, 180
Fang, J., & Zhang, L. 2010, A&A, 515, A20
Gaensler, B. M., Schulz, N. S., Kaspi, V. M., Pivovaroff, M. J., & Becker, W. E. 2003, ApJ, 588, 441
Gelfand, J. D., Slane, P. O., & Zhang, W. 2009, ApJ, 703, 2051
Hobbs, G. B., Edwards, R. T., & Manchester, R. N. 2006, MNRAS, 369, 655
Hobbs, G. B., Lyne, A. G., Kramer, M., Martin, C. E., & Jordan, C. 2004, MNRAS, 353, 1311
Kargaltsev, O., & Pavlov, G. G. 2008, in AIP Conf. Proc. 983, 40 Years of Pulsars: Millisecond Pulsars, Magnetars and More, ed. C. Bassa, Z. Wang, A. Cumming, & V. M. Kaspi (Melville, NY: AIP), 171
Lemiere, A., Slane, P., Gaensler, B. M., & Murray, S. 2009, ApJ, 706, 1269
Mattox, J. R., et al. 1996, ApJ, 461, 396
Pavlov, G. G., Kargaltsev, O., & Brisken, W. F. 2008, ApJ, 675, 683
Porter, T. A., & Strong, A. W. 2005, Proc. 29th Int. Cosmic Ray Conf., 4, ed. B. Sripathi Acharya et al. (Mumbai: Tata Institute of Fundamental Research), 77
Slane, P., Castro, D., Funk, S., Uchiyama, Y., Lemiere, A., Gelfand, J. D., & Lemoine-Goumard, M. 2010, ApJ, 720, 266
Spitkovsky, A. 2008, ApJ, 682, L5
Strong, A. W., Moskalenko, I. V., & Reimer, O. 2004, ApJ, 613, 962
Tanaka, S. J., & Takahara, F. 2010, ApJ, 715, 1248
Uchiyama, H., Matsumoto, H., Tsuru, T. G., Koyama, K., & Bamba, A. 2009, PASJ, 61, 189
Weltevrede, P., et al. 2010, PASA, 27, 64